RSC Advances

This article can be cited before page numbers have been issued, to do this please use: V. Elayappan, S. Angaiah, Z. Fei and P. Dyson, *RSC Adv.*, 2015, DOI: 10.1039/C5RA04944J.

ROYAL SOCIETY OF CHEMISTRY

www.rsc.org/advances

View Article Online
DOI: 10.1039/C5RA04944J

High performance dye sensitized solar cell based on electrospun poly(vinylidene fluoride-co-hexafluoropropylene)/Cobalt sulfide nanocomposite membrane electrolyte

Vijayakumar. E[a], Subramania. A[a,*], Zhaofu Fei[b], Paul J. Dyson[b]

[a]*Electrochemical Energy Research Lab, Centre for Nanoscience and Technology, Pondicherry University, Puducherry - 605 014, India.*

[b]*Institut des Sciences et Ingénierie Chimiques, Ecole Polytechnique Fédérale de Lausanne (EPFL) CH-1015, Lausanne, Switzerland.*

*(*Corresponding Author E-mail: a.subramania@gmail.com)*

Fax: (+91) 413-2655 348 Phone: (+91) 413-2654612.

ABSTRACT

Different weight percentage (1, 2 and 3wt%) of cobalt sulfide incorporated (CoS) incorporated electrospun poly(vinylidene fluoride-co-hexafluoropropylene) (PVdF-HFP) nanocomposite membranes were prepared by electrospinning technique. The surface morphology, crystallinity, porosity and electrolyte uptake of the electrospun nanocomposite membranes were examined. The prepared electrospun PVdF-HFP/CoS nanocomposite membranes (esCPM) were activated by ionic liquid electrolyte containing 0.5M LiI, 0.05M I_2 and 0.5M 4-tert butylpyridine, 0.5M 1-Butyl-3-methylimidazolium iodide in acetonitrile to obtain electrospun PVdF-HFP/CoS nanocomposite membrane electrolytes (esCPMEs). The uniformly dispersed CoS nanoparticles increase the charge transport and facilitate the diffusion of redox couple in the electrolyte system. The electrochemical characteristics of dye-sensitized solar cell (DSSC) depends on the amount of CoS incorporated in esCPME was also studied in detail. The photovoltaic performance of DSSC assembled using 1wt% of CoS incorporated esCPME was measured and it was found to be 7.34%, which is higher than that assembled using esPME (6.42%).

KEYWORDS: Electrospinning, Dye-sensitized solar cell, Cobalt sulfide, Nanocomposite membrane electrolyte.

View Article Online
DOI: 10.1039/C5RA04944J

INTRODUCTION

Dye-sensitized solar cells (DSSCs) can serve as the promising mainstream renewable energy resource because of their clean high energy efficiency and low cost. Since the first report by Gratzel, the overall efficiency as high as 11% has been achieved with liquid electrolytes through various works. However technical problems such as electrolyte leakage, evaporation of solvent, high temperature instability and flammability limit their long term performances. Among the alternatives such as inorganic or organic hole conductors[1], ionic liquids [2], polymer gel electrolytes [3,4] stand out because of their excellent properties such as easy fabrication, low cost, and good stability. But, the gel network hinders the charge transport in gel electrolytes to certain extent. Also, the gel electrolytes suffer from low electrolyte loading per unit volume and consequently low ionic conductivity. In order to rectify this negative influence of polymer gel electrolytes, electrospun polymer membrane electrolytes have been investigated for DSSC applications. These polymer electrolytes have several advantages over their liquid counter parts, such as no internal shorting, leakage of electrolytes and non-combustible reaction products at the electrode surface than in liquid electrolytes. Till date, polymer hosts such as poly(ethyleneoxide) (PEO), poly(propylene oxide) (PPO), poly(acrylonitrile) (PAN), poly(methyl methacrylate) (PMMA), poly(vinyl chloride) (PVC), poly(vinylidene fluoride) (PVdF), poly(vinylidene fluoride-hexafluoro propylene) (PVdF-HFP), etc., have been used for DSSC applications [5]. Recent advances have proved that nanostructured metal chalcogenides (MCs) such as FeS_2, CoS, NiS are great potential materials for energy conversion and storage utilization because of their unique physical and chemical properties [6–12]. Following that, we have described the promising applications of MCs in the field of DSSCs. The advantages of using MCs are higher electric conductivity, and shorter path length for the transport of electrons.

In the present work, we have developed the cobalt sulfide (CoS) incorporated esCPME due to the superior electrocatalytic activity of CoS. The electrospinning is the top-

View Article Online
DOI: 10.1039/C5RA04944J

down, simple, versatile and cost effective approach allowing the fabrication of nanofibers with high degree of reproducibility for various applications such as Dye sensitized solar cells, supercapacitors, Li-ion batteries, nano-filters etc., [13–20]. The electrospun polymer membranes have their own unique properties such as high porosity, large surface area, fully interconnected pore structure with sufficient mechanical strength and also have three-dimensional network structure. They offer the advantage of cohesive properties of the gel polymer electrolyte along with the diffusive nature of the liquid electrolyte due to its interconnected pores that can easily entrap a large quantity of liquid electrolyte which improve the interfacial contact of both electrodes with electrolyte[21]. The room temperature ionic liquids are promising alternatives to volatile electrolyte due to their unique properties such as negligible vapor pressure, excellent electrochemical and thermal stability as well as the high ionic conductivity [22]. The fluorinated polymers are known to be photochemically stable even in the presence of TiO_2 and Pt. The higher conductivity of PVdF-HFP films is attributed to the higher amorphicity as there are two randomly mixed monomers providing the mobile ions more free [23]. Thus, to improve the interfacial and ionic conductivity of electrospun polymer membrane electrolyte, CoS nanoparticles are introduced into the electrospun membrane. The encapsulation of nanoparticles addresses a vast range of problems such as low ionic conductivity, interfacial stability, mechanical strength dimensional and thermal stabilities. The addition of CoS nanoparticles will increase further the amorphous content, thereby increasing the electrolyte uptake. Also, the CoS nanoparticles enhance the diffusion coefficient of I_3^- and also reduce the charge recombination at the TiO_2/electrolyte interface. The significance of this study lies in improving the kinetics of ion transport and thereby the electrochemical activity of the electrospun membrane electrolyte. By this approach, the electrospun polymer membrane electrolyte would increase the photoconversion efficiency of DSSC.

View Article Online
DOI: 10.1039/C5RA04944J

EXPERIMENTAL

Materials

Acetone and N,N'-dimethylacetamide were procured from Merck India Ltd. Lithium iodide, iodide, 4-*tert*-butylpyridine and acetonitrile were procured from Sigma Aldrich and PVdF-HFP from Arkema (Kynar flex 2801). All these chemicals are analytical grade and used as received without any further purification. The cobalt sulfide nanoparticles were prepared by a simple hydrothermal method. In this method, 3 mmol $CoCl_2.6H_2O$ solution in deionized water was added to the 3 mmol L-cysteine solution in deionized water with constant and vigorous stirring. After 15 min, the resulting mixture was heated and maintained at 190°C for 6 h in an autoclave. The resulting product was then washed and vacuum dried at 50°C for overnight[24].

Preparation of electrospun PVDF-HFP/CoS composite membrane

The different weight percentage of CoS (1wt %, 2wt %, 3wt %) were added to 16 wt% solution of PVdF-HFP in a mixture of acetone/N,N'-dimethyl acetamide (7:3 wt%). The electrospinning was carried out at 19 KV and the distance between the collector and tip of the syringe was kept at 12cm. The polymer solution was supplied to the stainless steel needle (27 G) using a syringe pump at the flow rate of 0.5 ml/h. The thickness of the membrane was controlled to 30 µm. Finally, the prepared nanofibrous composite membranes was vacuum dried at 80°C for 12 h to remove residual solvent. The thickness of esCPMs was reduced from ca. 30 to 20 µm by hot pressing[21].

Characterization of esCPM

The surface morphology of esCPM was examined by field emission scanning electron microscopy (FE-SEM; Model: JSM-7600F). The structural characterization of different wt% of CoS incorporated esCPM was studied by X-ray diffraction technique (Rigaku, Ultima IV) with nickel-filtered Cu-Kα radiation in a range from 20° to 80° with an increment of 0.05°. The fourier transform infrared (FT-IR) spectra were recorded for the esPM, CoS, esCPM

View Article Online
DOI: 10.1039/C5RA04944J

(Thermo Nicolet, Model:6700). Thermal behavior of esCPMs was studied by differential scanning calorimetry (DSC) at a heating rate of 10°C/min under a nitrogen atmosphere over the temperature range of 30 °C - 280 °C (TA Instruments; Model: Q600 SDT).

The crystallinity (X_c) of esCPMs was calculated as follows [25];

$$X_c(\%) = \frac{\Delta H_m^{sample}}{\Delta H_m^*} \times 100 \quad (1)$$

where, ΔH_m^{sample} is the heat of melting of the sample and ΔH_m^* is the crystalline melting heat of PVdF, 104.7 J/g.

The porosity (%) of esCPMs was measured by immersing the nanocomposite membranes in 1-butanol for 2 hour. The porosity (P) was calculated using the following equation[26];

$$P = \frac{m_a / \rho_a}{m_a / \rho_a + m_p / \rho_p} \quad (2)$$

where, 'm_a' is the weight of esCPMs after impregnation with 1-butanol, 'm_p' is the weight of esCPM before impregnation with 1-butanol, and 'ρ_a' and 'ρ_p' are density of 1-butanol and the dried esCPM, respectively.

To measure the electrolyte uptake of esCPMs, the nanocomposite membranes were soaked in the ionic liquid electrolyte for 24 h. After activation, the electrolyte membranes were taken out from the electrolyte solution and an excess of electrolyte on the electrospun membrane was wiped off by whatman filter paper. Electrolyte uptake (U) was estimated using the formula [5];

$$U(\%) = [(m - m_\circ) / m_\circ] \times 100 \quad (3)$$

where, 'm' and 'm_o' are the mass of wet and dry esCPMs, respectively.

View Article Online
DOI: 10.1039/C5RA04944J

The leakage of the electrolyte was calculated using the equation [4];

$$R = \frac{M_{PE}}{M_{PE,saturated}} \quad (4)$$

where, *R* is the relative absorption ratio of the liquid electrolyte, $M_{PE,saturated}$ is the mass of the polymer electrolyte when the electrospun membrane is fully saturated with the liquid electrolyte, and M_{PE} is the mass of the electrospun membrane electrolyte after a time interval when the saturated electrospun membrane electrolyte is squeezed by pressing it between two filter papers.

The electrochemical impedance spectra and Tafel polarization measurements verify the electrochemical activities. The different weight percentage of CoS incorporated esCPMs were soaked in the ionic liquid electrolyte to form their corresponding esCPMEs. The ionic conductivity of the resultant esCPMEs (σ) was measured by sandwiching the nanocomposite membrane electrolyte in between two stainless steel blocking electrodes using AC-impedance technique (Biologic, Model: VSP) at 25 ˚C. The ionic conductivity (σ) of the electrospun PVDF-HFP nanocomposite membrane electrolytes was calculated using the equation [23];

$$\sigma = \ell / RA \quad (5)$$

where, ℓ is the polymer membrane thickness, *A* is the area of the esCPME and *R* is the bulk resistance. The bulk resistance could be obtained from the complex impedance plot. The frequency limit was set between 1 mHz and 100 KHz with AC amplitude of 10 mV. The thickness (ℓ) of the esCPM was determined using a digital micrometer and was found to be 20 μm. The area (A) of the polymer membrane was 1 cm^2.

The Tafel polarization measurement were carried out using symmetric cells consisting of FTO/Pt/esCPMEs/Pt/FTO to reconfirm the electrocatalytic activity of esCPME [27].

Fabrication of dye-sensitized solar cells (DSSCs)

The DSSCs were assembled as per the earlier reports by sandwiching a slice of esCPME in between a dye-sensitized TiO_2 photoanode and Pt counter electrode [23]. The dye

View Article Online
DOI: 10.1039/C5RA04944J

adsorbed titania photoanode and Pt counter electrode were assembled using 60 μm thick hot melt thermoplastic sealer (Surlyn). A drop of the electrolyte solution containing 0.5 M LiI, 0.05 M I_2 and 0.5 M 4-tertbutylpyridine and 0.5 M 1-butyl-3-methylimidazoliun iodide in acetonitrile [21] was introduced into the clamped electrodes through one of two small holes drilled in the counter electrode. The DSSC based on esPME were also assembled following the same procedure for comparison.

Photovoltaic Performance of DSSCs

The photovoltaic performance of DSSCs were measured using a calibrated AM 1.5 solar simulator (Newport, Oriel instruments, Model: 67005) with a light intensity of 100 mW cm^{-2} and a computer controlled digital source meter (Keithley, Model: 2420). I-V measurements were carried out on the DSSCs after an aging period of 24 h. The assembled DSSCs were stored in a desiccator and the electrochemical measurements were conducted for every 48 h to study their long term stability. The photoelectrochemical parameters, i.e., the fill factor (FF) and light-to-electricity conversion efficiency (η) were calculated with the following equations [28]:

$$\eta\,(\%) = \frac{V_{\max} J_{\max}}{P_{in}} \times 100 = \frac{V_{oc} J_{sc} FF}{P_{in}} \times 100 \qquad (6)$$

$$FF = \frac{V_{\max} J_{\max}}{V_{oc} J_{sc}} \qquad (7)$$

where, J_{sc} is the short-circuit current density (mA cm^{-2}), V_{oc} is the open-circuit voltage (V), P_{in} is the incident light power (mW cm^{-2}), and J_{max} and V_{max} are the current density (mA cm^{-2}) and voltage (V) in the *J-V* curves, respectively at the point of maximum power output. All the fabrication steps and characterization measurements were carried out in an ambient environment without any protective atmosphere. The photovoltaic parameter values were made by taking the average values of three DSSCs for each system.

View Article Online
DOI: 10.1039/C5RA04944J

RESULTS AND DISCUSSION

Characterization for esCPMs and esCPMEs

The FE-SEM image of the prepared esPM and esCPM (1 wt%) are shown in Fig. 1(a & b). The FE-SEM image of the prepared esPM and esCPM are shown in Fig. 1(a & b). It can be seen from Fig. 1(a) that the esCPM has a three-dimensional network with fully interconnected pores structure that capable of entrapping large amount of ionic liquid electrolyte in their pores which favorable for the transportation of redox couple resulting in the improvement of ionic conductivity. In Fig. 1(b), the bubble like structure observed is due to CoS nanoparticles incorporated in host esCPM. This esCPM has sufficient mechanical strength due to its three dimensional network structure with cross linking points [23]. The esCPM (average diameter of the fibers is 300-350 nm) has a maximum porosity, electrolyte uptake and less leakage are 94 %, 410 % and 0.2, respectively. The increase in the electrolyte uptake upon the addition of CoS nanoparticles is mainly due to increase in the porosity on account of increase in surface roughness. Also, the CoS fillers decreases the degree of crystallinity that provide a large free volume and many free surface sites able to trap ionic liquid electrolyte which increase further the ionic conductivity as well as the electrochemical performance. However, beyond the optimum concentration of CoS, the blocking effect is caused by the aggregation of CoS nanoparticles which decreases the porosity thereby reducing the ability of electrolyte uptake.

The FT-IR spectra of PVdF-HFP, CoS and esCPM (1 wt%) are shown in Fig. 2. The peaks at about 1395, 867 and 485 cm^{-1} are due to the C-F_2 bending, wagging and stretching vibrations and peak at 1185 is due to the C-C bond of PVdF. It is clear that the spectrum of PVdF-HFP contains peak at 611, 872, 1064, 1180 and 1400 cm^{-1} that corresponds to vinylidene, CH_2 wagging of the vinylidene band, -C-F- stretching, scissoring and bending vibration of the vinyl group, respectively. The peaks at 680 cm^{-1} and 550 cm^{-1} correspond to twisting in vinyl group. For cobalt sulfide nanoparticles, the appearance of band at 474.4 cm^{-}

View Article Online
DOI: 10.1039/C5RA04944J

^{1} and 1115 cm^{-1} corresponds to the S-O modes. The peak at 1527 cm^{-1} is due to the -OH stretching. No shift in peaks are observed in esCPM indicating that there is no conjugate bonds or interaction between PVDF-HFP and CoS nanoparticles. It reveals that the CoS nanoparticles are incorporated in the host esCPM and there is no complex formation between PVdF-HFP and CoS.

The variation in crystallinity of PVdF-HFP owing to the addition of different weight percentage of CoS nanoparticles are studied by X-ray diffraction. The XRD patterns for PVdF-HFP powder, CoS, esPM and esCPMs are shown in Fig. 3. The diffraction peaks of CoS nanoparticles are matched with standard XRD pattern (ICSD No. 029305). No impurity peaks were observed indicates the formation of pure CoS nanoparticles [29]. In the XRD pattern of PVdF-HFP, the major peaks at 18.2° and 20.0° corresponds to (100) and (020) crystalline phase, respectively. It is observed that the intensity of peak weakened for electrospun PVDF-HFP that makes the migration of polymer chain free [30]. The intensity these peaks reduced considerably with increase in the addition of CoS which indicates the addition of CoS considerably reduced its partial crystallinity to amorphous. The decrement in peak intensity suggests an increase in the degree of amorphicity that helps in the migration of ions in the electrolyte system, which is responsible for the enhancement of ionic conductivity. Also, the decrease in the crystallinity indicates the better dispersion of CoS nanoparticles in the electrospun membrane. The lowest crystallinity is found for 1wt% of CoS incorporated esCPM. However, on increasing the CoS content beyond 1wt%, they tend to agglomerate and create a blocking effect on the mobility of redox couple, hereby increased the crystallinity and deteriorate the polymer chain movement. Thus, 1wt% of CoS incorporated esCPME provided high ionic conductivity and thereby increased the photovoltaic performance.

Fig. 4 shows the DSC thermograms of esPM and 1wt% of CoS incorporated esCPM. The addition of CoS nanoparticles increase the amorphous phase of the host. It is observed that 1wt% of CoS incorporated esCPM have more amorphous content than the esPM which is

View Article Online
DOI: 10.1039/C5RA04944J

realized from the XRD results. In the esCPME, the solar conversion efficiency strongly depends on the ionic conductivity. On incorporation of 1 wt% of CoS, the amorphous content increased considerably. The amorphous content has high ionic mobility and thereby enhanced the ionic conductivity. The percentage of crystallinity is calculated using equation 1. The 1wt% of CoS incorporated esCPM has the lower crystallinity (22.84%) than that of esPM (31.97%), which ensure its higher electrolyte uptake that leads to enhance the charge carriers mobility and thereby increased the ionic conductivity.

The ionic conductivity of different weight percentage of CoS incorporated esCPMEs are calculated from the bulk resistance obtained from complex impedance measurements at ambient temperature is given in Table 1 (Fig. 5). The inclusion of CoS nanoparticles improved the amorphicity content and provides the diffusion path in the electrospun membrane. Thus, an excellent improvement attributed to esCPME is due to high amorphicity content, which endorses the dissociation of charge carriers from the interactive bonds and provides a favorable condition for the fast migration of iodide and triiodide ions to favor an improvement in the conductivity of ionic liquid. The esCPME is thought to comprise a solid fibrous phase, an amorphous swollen fibrous phase and a liquid phase in its pores. This indicates that the partial swelling of the polymer fibers with a large surface area significantly contribute to increase in stability of the electrolyte under electrochemical environments, although the ionic conduction occurred mainly through the entrapped liquid electrolyte in a fully interconnected pore structure. The liquid electrolyte which accumulated in between the interconnected pores present in the esCPM to act as gel like as well as liquid electrolytes.

The increase in ionic conductivity with the addition of CoS is related to both the generation of free volume at the interface of inorganic materials and the surface interactions with the inorganic iodide. The CoS provides increase in molecular ordering and ionic conductivity as well as the formation of diffusion path for the redox species thereby increases the electrochemical activity of CoS incorporated esCPMEs. The reduction in the ionic

View Article Online
DOI: 10.1039/C5RA04944J

conductivity on increasing the CoS content beyond 1wt% is due to the agglomeration of CoS nanoparticles. The agglomeration makes the polymer membrane stiffer and thereby obstructs the segmental motion of the polymer chains that hinder the transportation of the charge carriers. The hindrance in charge transportation (blocking effect) decreases the ionic conductivity. Fig. 6 shows the illustration of formation of esCPME and the blocking effect due the agglomeration of CoS beyond its optimum concentration. The ionic conductivity of 1 wt% of CoS incorporated esCPME has the maximum value of 36.43×10^{-3} S cm^{-1}. The PCE of DSSC depends on the ionic conductivity of esCPME. Thus, 1wt% of CoS incorporated esCPME may have high PCE.

Fig. 7 shows the Tafel curves of different wt% of CoS incorporated esCPMEs. The slope of the polarization zone represents the charge transfer resistance (R_{ct}), which is inversely proportional to the exchange current density (J_0). It is an important indicator for assessing the electrochemical reaction kinetics. The steep slope of Tafel zone has a large J_0 and small R_{ct} values. It is observed that 1wt% of CoS incorporated esCPME has larger slope and higher J_{lim} than that of the other weight percentages. The values of J_0 can be obtained from the intersection of linear cathodic and anodic region and the values of J_{lim} can be obtained by drawing a straight line towards the current density axis from a point of both anodic and cathodic region in the Tafel polarization curves. This results indicate the higher catalytic activity towards triiodide couple and the higher diffusion velocity of facial redox reaction in esCPME [31].

Photovoltaic performance of DSSCs

The photocurrent density-voltage (J-V) curves were obtained at a light intensity of 100 mW cm^{-2} under the standard global AM 1.5 irradiation are shown in Fig. 8 (Table 2). The DSSCs assembled using esCPME (1wt% CoS) provides power conversion efficiency of 7.34% higher than that of esPME (6.42%). The increasing amorphous nature of the esCPME on addition of CoS nanoparticles, improve the penetration of esCPME into porous TiO_2

View Article Online
DOI: 10.1039/C5RA04944J

electrode, thereby decreasing the interfacial recombination of electrons, which leads to higher in J_{sc} and fill factor values. Moreover, the electrocatalytic activity of esCPME reduces the over potential which in turn increases the V_{oc} value. The increasing amorphous nature of esCPME on the addition of CoS, improve the penetration of esCPME into porous TiO_2 photoanode, thereby decreasing the interfacial recombination of electrons, which leads to increased J_{sc} and fill factor. Moreover, the electrocatalytic activity of esCPME reduces the over potential which in turn increases the V_{oc} value. Fig. 9 illustrates the mechanism of increased reaction kinetics of DSSC assembled using esCPME. At optimal concentration of CoS (1 wt%), the reaction kinetics increases and hence photovoltaic performance is also increased. This may be due to the direct conductive pathway of electrons provided by CoS nanoparticles and their electrocatalytic activity. However, further increase in the concentration of CoS, cause poor penetration of esCPME into TiO_2 photoanode due to stiffness caused by agglomeration and also direct contact of CoS nanoparticles which may form short circuit, that lead to the depletion of photovoltaic performance. The increment in values of Jsc values from 13.10 to 14.42 is mainly attributed to the low charge transfer resistance and higher electrocatalytic activity in the reduction of I_3^-/I^- electrolyte. Thus, the CoS incorporated esCPME ensured an effective charge transfer at the CE/electrolyte interface with lower recombination rate in the DSSC, which ultimately increased the PCE.

The stability of DSSCs assembled with both esPME and esCPME (1 wt%) was studied over a period of 30 days (Fig. 10). Both DSSCs retain ca. 99% of their initial value. Notably, no decay was observed in the overall PCE of both the DSSCs. This might be due to their three dimensional network with interconnected pores. These interconnected pores are able to trap the liquid electrolyte and consequently, the resulting esPME/esCPME appears to act as liquid as well as gel electrolytes. Thus, both the esPME and esCPME appears to promote interfacial contact between the dye-adsorbed TiO_2 electrode and the Pt counter electrode, which helps to give more stable photovoltaic performance.

View Article Online
DOI: 10.1039/C5RA04944J

CONCLUSIONS

The CoS incorporated esCPMs were prepared successfully by electrospinning technique and compared with esPM. Their surface morphology, crystallinity, thermal behavior, % porosity and % electrolyte uptake were studied. They were then activated by a liquid electrolyte and their ionic conductivity and Tafel polarization measurements were made. The esCPME (1 wt% of CoS) shows higher ionic conductivity of 36.43×10^{-3} S cm^{-1}. The 1wt% CoS incorporated esCPME showed superior photovoltaic performance. The increased active surface area of esCPME by the incorporation of CoS could promote electrocatalytic activity of I_3^- reduction and the total current for I_3^- / I^- redox reaction, which enhanced the Jsc value of the DSSC. Thus, DSSC assembled using 1wt% of CoS incorporated esCPME shows an improved PCE of 7.34%, which is higher than that assembled using esPME (6.42%).

ACKNOWLEDGEMENTS

The authors gratefully acknowledge the CSIR (Ref. No.01/2359/10/EMR-II) New Delhi for the financial support and also the CIF of Pondicherry University for extending the instrumentation facilities.

REFERENCES

1. I.-K. Ding, J. Melas-Kyriazi, N.-L. Cevey-Ha, K. G. Chittibabu, S. M. Zakeeruddin, M. Grätzel, and M. D. McGehee, *Org. Electron.*, 2010, **11**, 1217–1222.

2. P. Wang, S. M. Zakeeruddin, J.-E. Moser, and M. Grätzel, *J. Phys. Chem. B*, 2003, **107**, 13280–13285.

3. S. Cetiner, F. Kalaoglu, H. Karakas, and A. Sezai Sarac, *Fibers Polym.*, 2011, **12**, 151–158.

4. N. Angulakshmi and A. M. Stephan, *Electrochim. Acta*, 2014, **127**, 167–172.

5. J. Zhao, S.-G. Jo, and D.-W. Kim, *Electrochim. Acta*, 2014, **142**, 261–267.

6. Q.-H. Huang, T. Ling, S.-Z. Qiao, and X.-W. Du, *J. Mater. Chem. A*, 2013, **1**, 11828.

7. Y.-C. Wang, D.-Y. Wang, Y.-T. Jiang, H.-A. Chen, C.-C. Chen, K.-C. Ho, H.-L. Chou, and C.-W. Chen, *Angew. Chem. Int. Ed. Engl.*, 2013, **52**, 6694–8.

View Article Online
DOI: 10.1039/C5RA04944J

8. H. Sun, D. Qin, S. Huang, X. Guo, D. Li, Y. Luo, and Q. Meng, *Energy Environ. Sci.*, 2011, **4**, 2630.

9. Z. Ku, X. Li, G. Liu, H. Wang, Y. Rong, M. Xu, L. Liu, M. Hu, Y. Yang, and H. Han, *J. Mater. Chem. A*, 2013, **1**, 237.

10. J.-Y. Lin, J.-H. Liao, and T.-C. Wei, *Electrochem. Solid-State Lett.*, 2011, **14**, D41.

11. J.-Y. Lin and J.-H. Liao, *J. Electrochem. Soc.*, 2012, **159**, D65.

12. X. Miao, K. Pan, G. Wang, Y. Liao, L. Wang, W. Zhou, B. Jiang, Q. Pan, and G. Tian, *Chemistry*, 2014, **20**, 474–82.

13. X. Zhang, P. Suresh Kumar, V. Aravindan, H. H. Liu, J. Sundaramurthy, S. G. Mhaisalkar, H. M. Duong, S. Ramakrishna, and S. Madhavi, *J. Phys. Chem. C*, 2012, **116**, 14780–14788.

14. X. Zhang, H. Liu, S. Petnikota, S. Ramakrishna, and H. J. Fan, *J. Mater. Chem. A*, 2014, **2**, 10835–10841.

15. Z. Xiang, B. R. S. Rajaraman, H. Liu, and S. Ramakrishna, *RSC Adv.*, 2014, 28987–29011.

16. X. Zhang, V. Thavasi, S. G. Mhaisalkar, and S. Ramakrishna, *Nanoscale*, 2012, **4**, 1707.

17. S. Homaeigohar and M. Elbahri, *Materials*, 2014, **7**, 1017–1045.

18. S. Sundarrajan, K. Luck, S. Huat, and S. Ramakrishna, *Procedia Eng.*, 2014, **75**, 159–163.

19. K. Yoon, K. Kim, X. Wang, D. Fang, B. S. Hsiao, and B. Chu, *Polymer*, 2006, **47**, 2434–2441.

20. S. Ramakrishnan, M. Dhakshnamoorthy, E. J. Jelmy, R. Vasanthakumari, and N. K. Kothurkar, *RSC Adv.*, 2014, **4**, 9743.

21. Vijayakumar E, Subramania A, Z. Fei, and P. J. Dyson, *J. Appl. Polym. Sci*, 2015, **132**, 42032 (1–7).

22. Y.-L. Lee, Y.-J. Shen, and Y.-M. Yang, *Nanotechnology*, 2008, **19**, 455201.

23. A. R. S. Priya, A. Subramania, Y.-S. Jung, and K.-J. Kim, *Langmuir*, 2008, **24**, 9816–9.

24. S.-J. Bao, C. M. Li, C.-X. Guo, and Y. Qiao, *J. Power Sources*, 2008, **180**, 676–681.

25. A. Subramania, N. T. K. Sundaram, A. R. S. Priya, and G. V. Kumar, *J. Memb. Sci.*, 2007, **294**, 8–15.

26. J. Hao, Q. Xiao, G. Lei, Z. Li, and L. Wu, *Electrochim. Acta*, 2014, **125**, 450–456.

View Article Online
DOI: 10.1039/C5RA04944J

27. S. Yuan, Q. Tang, B. He, and P. Yang, *J. Power Sources*, 2014, **254**, 98–105.

28. A. Subramania, E. Vijayakumar, N. Sivasankar, A. R. Sathiya Priya, and K.-J. Kim, *Ionics*, 2013, **19**, 1649–1653.

29. G. Panthi, N. A. M. Barakat, K. Abdelrazek, A. Yousef, K. Jeon, and H. Yong, *Ceram. Int.*, 2013, **39**, 1469–1476.

30. R. Miao, B. Liu, Z. Zhu, Y. Liu, J. Li, X. Wang, and Q. Li, *J. Power Sources*, 2008, **184**, 420–426.

31. Q. Li, X. Chen, Q. Tang, H. Cai, Y. Qin, B. He, M. Li, S. Jin, and Z. Liu, *J. Power Sources*, 2014, **248**, 923–930.

View Article Online
DOI: 10.1039/C5RA04944J

Figure Captions

Fig. 1 FE-SEM photograph of a) esPM and b) 1wt% of CoS incorporated esCPM

Fig. 2 FTIR spectra of esPM, CoS and 1wt% of CoS incorporated esCPM

Fig. 3 XRD patterns of PVdF-HFP powder, CoS and different wt% of CoS incorporated esCPMs

Fig. 4 DSC analysis of esPM and 1wt% of CoS incorporated esCPME.

Fig. 5 Nyquist plots for different wt% of CoS incorporated esCPMEs on ionic conductivity

Fig. 6 Illustration of formation of esCPME and the blocking effect due to the agglomeration of CoS beyond its optimum concentration.

Fig. 7 Tafel polarization curves of the symmetrical cells assembled with different wt% of CoS incorporated esCPME

Fig. 8 Photocurrent density-voltage (J-V) curves for DSSC based on (a) esPME (b) 1wt% of CoS incorporated esCPME.

Fig. 9 Illustrates the mechanism of increased reaction kinetics of DSSC assembled using esCPME.

Fig. 10 Normalized efficiency of a) esPME and b) 1wt% of CoS incorporated esCPME.

View Article Online
DOI: 10.1039/C5RA04944J

Tables

Table 1 Influence of different wt% of CoS incorporated esCPMEs on ionic conductivity

Electrolyte	Ionic conductivity ($\times 10^{-3}$ S cm^{-1})	U (%)	P (%)
esPME	5.83	340	84
esCPME (1 wt% CoS)	36.43	410	94
esCPME (2 wt% CoS)	29.17	392	90
esCPME (3 wt% CoS)	16.22	376	87

Table 2 Photovoltaic performances of DSSCs based on esPME and 1wt% of CoS incorporated esCPME .

Electrolyte	Jsc (mA cm^{-2})	Voc (V)	FF	Efficiency (%)
esPME	13.10	0.71	69	6.42
esCPME (1wt% CoS)	14.42	0.73	70	7.34

View Article Online
DOI: 10.1039/C5RA04944J

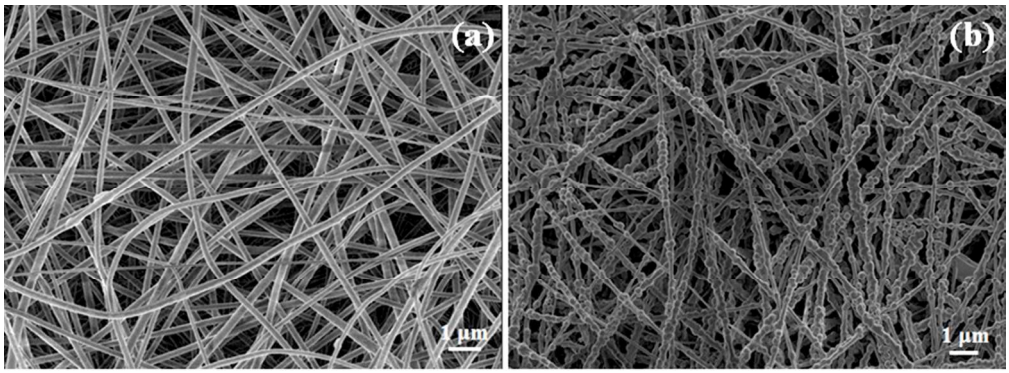

Fig. 1 FE-SEM photograph of a) esPM and b) 1wt% of CoS incorporated esCPM

View Article Online
DOI: 10.1039/C5RA04944J

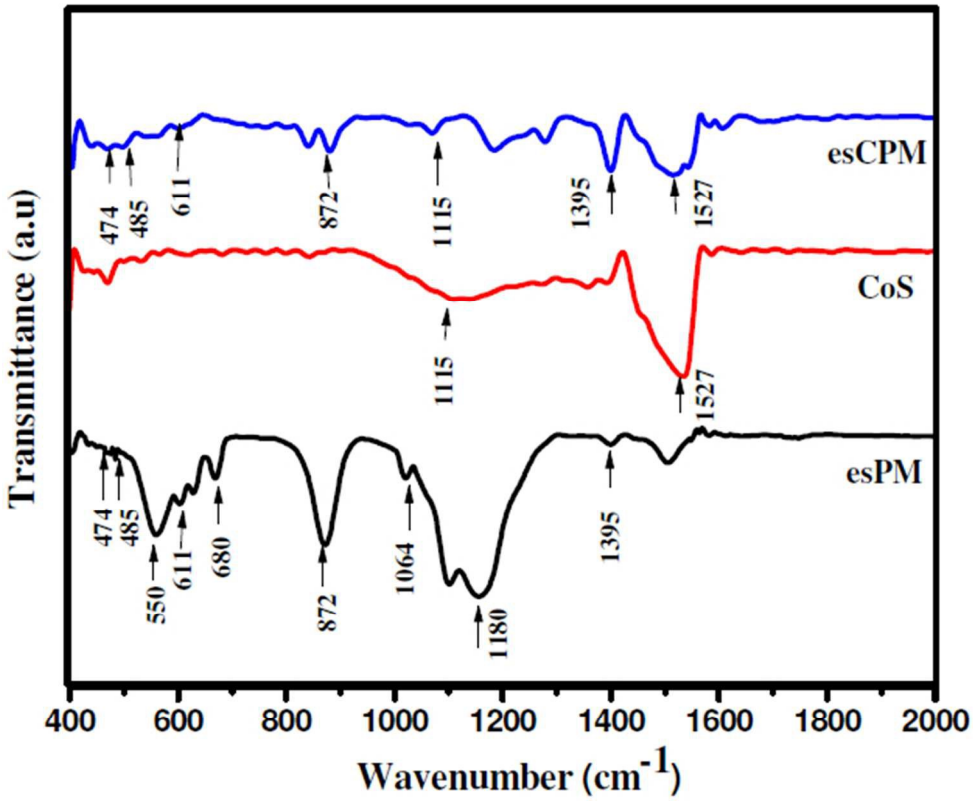

Fig. 2 FTIR spectra of esPM, CoS and 1wt% of CoS incorporated esCPM

View Article Online
DOI: 10.1039/C5RA04944J

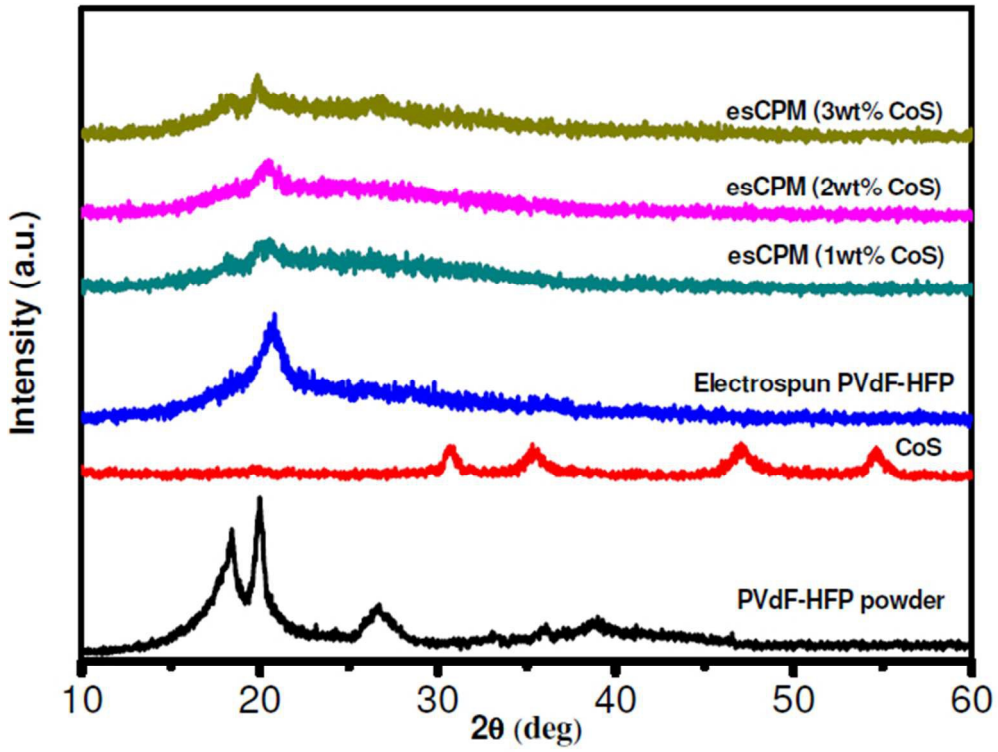

Fig. 3 XRD patterns of PVdF-HFP powder, CoS and different wt% of CoS incorporated esCPMs

View Article Online
DOI: 10.1039/C5RA04944J

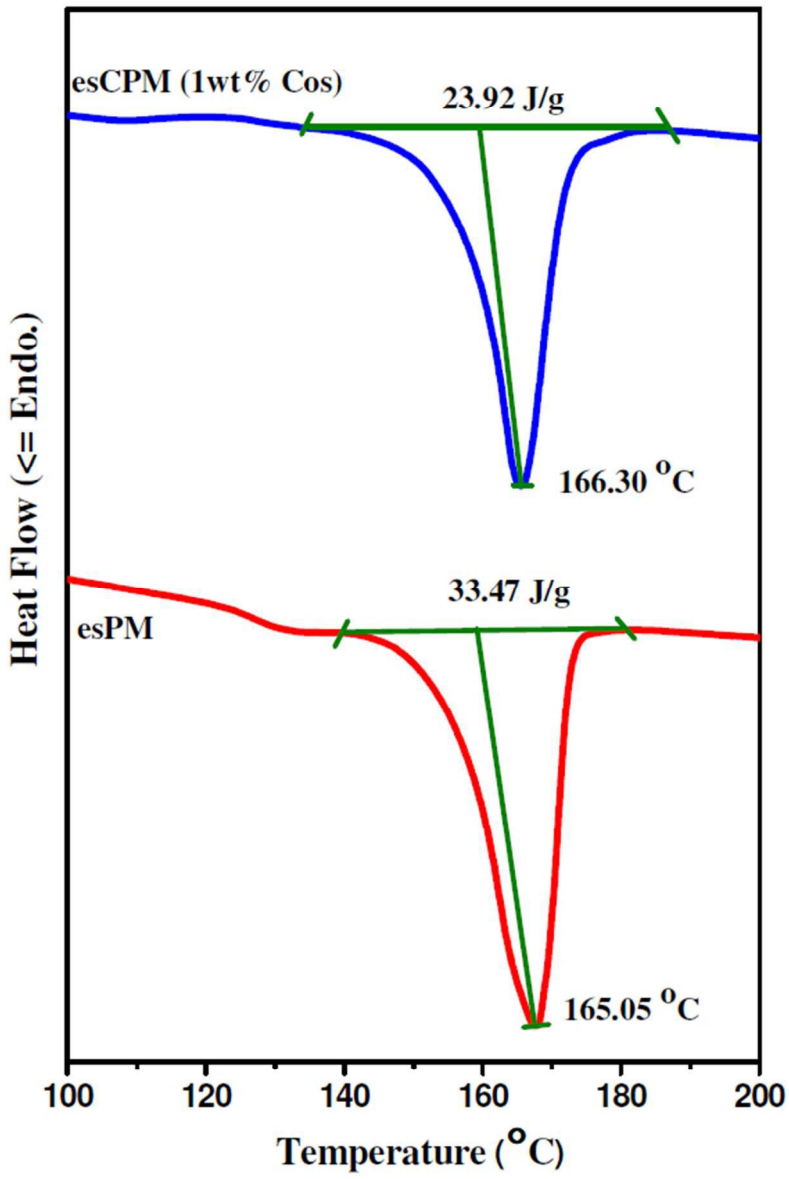

Fig. 4 DSC analysis of esPM and 1wt% of CoS incorporated esCPME.

View Article Online
DOI: 10.1039/C5RA04944J

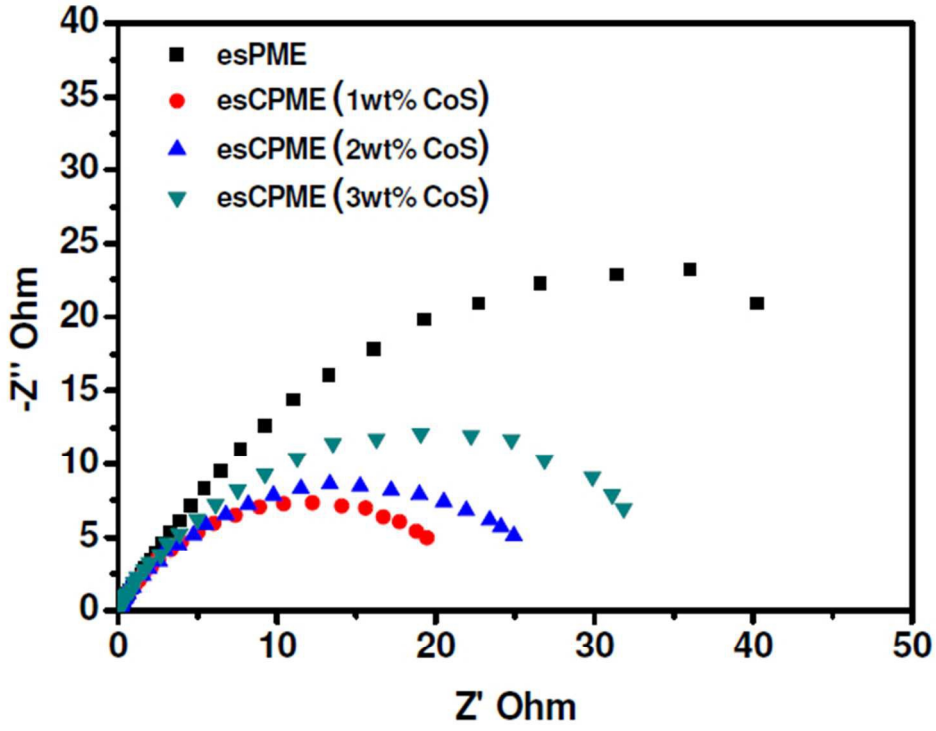

Fig. 5 Nyquist plots for different wt% of CoS incorporated esCPMEs on ionic conductivity

View Article Online
DOI: 10.1039/C5RA04944J

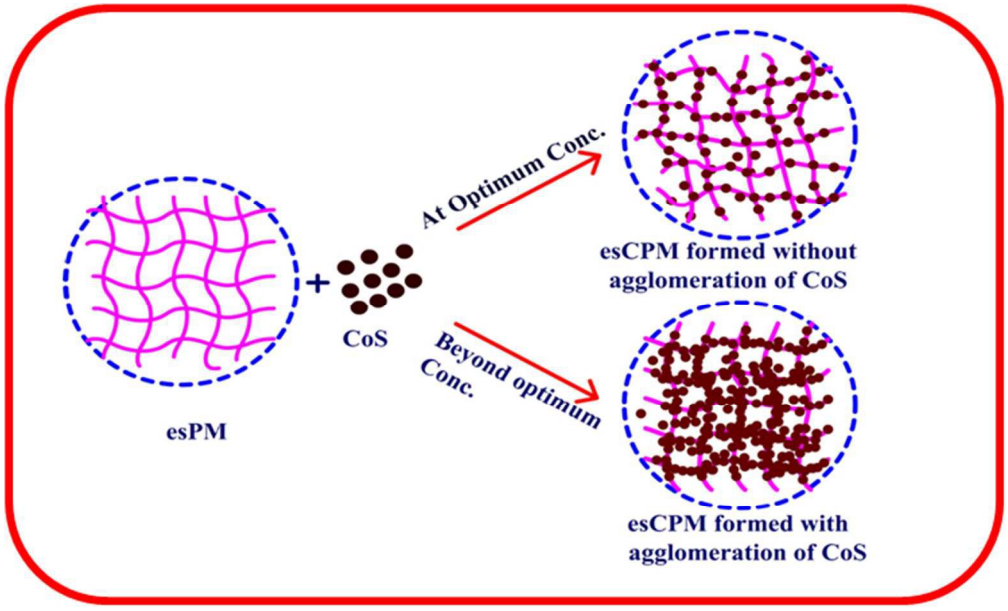

Fig. 6 Illustration of formation of esCPME and the blocking effect due to the agglomeration of CoS beyond its optimum concentration.
62x37mm (300 x 300 DPI)

View Article Online
DOI: 10.1039/C5RA04944J

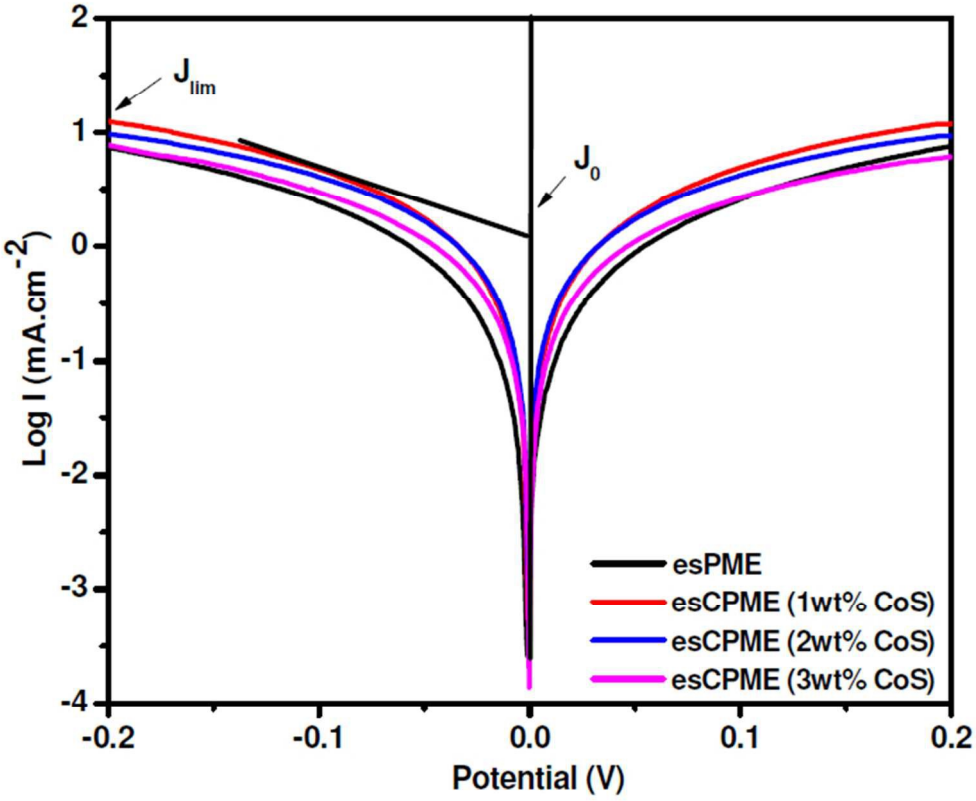

Fig. 7 Tafel polarization curves of the symmetrical cells assembled with different wt% of CoS incorporated esCPME

View Article Online
DOI: 10.1039/C5RA04944J

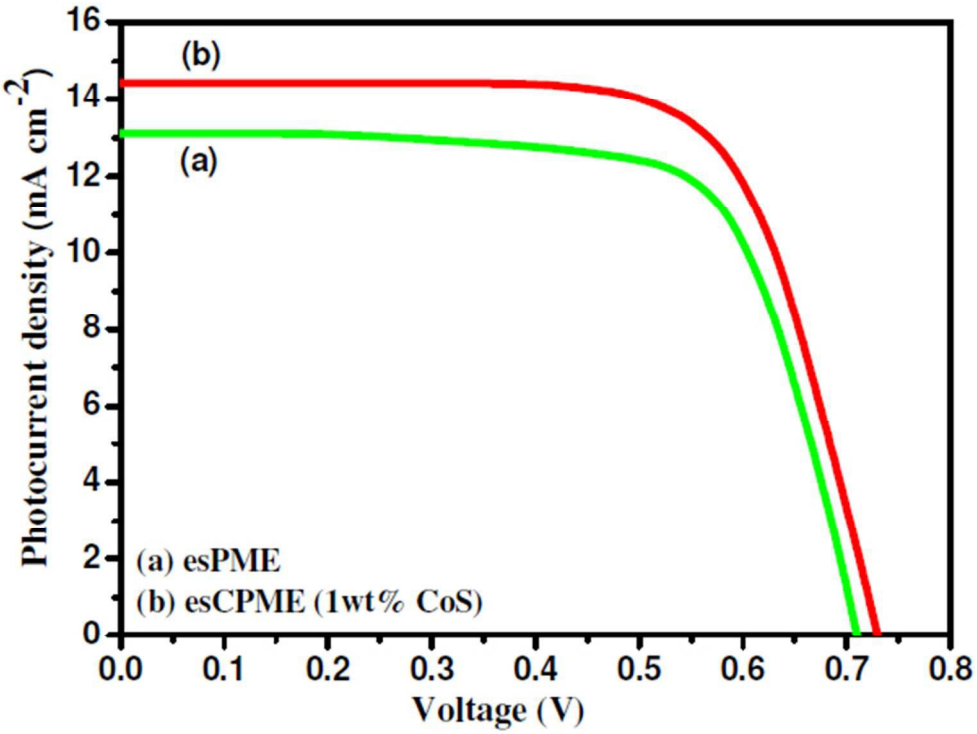

Fig. 8 Photocurrent density-voltage (J-V) curves for DSSC based on (a) esPME (b) 1wt% of CoS incorporated esCPME.

View Article Online
DOI: 10.1039/C5RA04944J

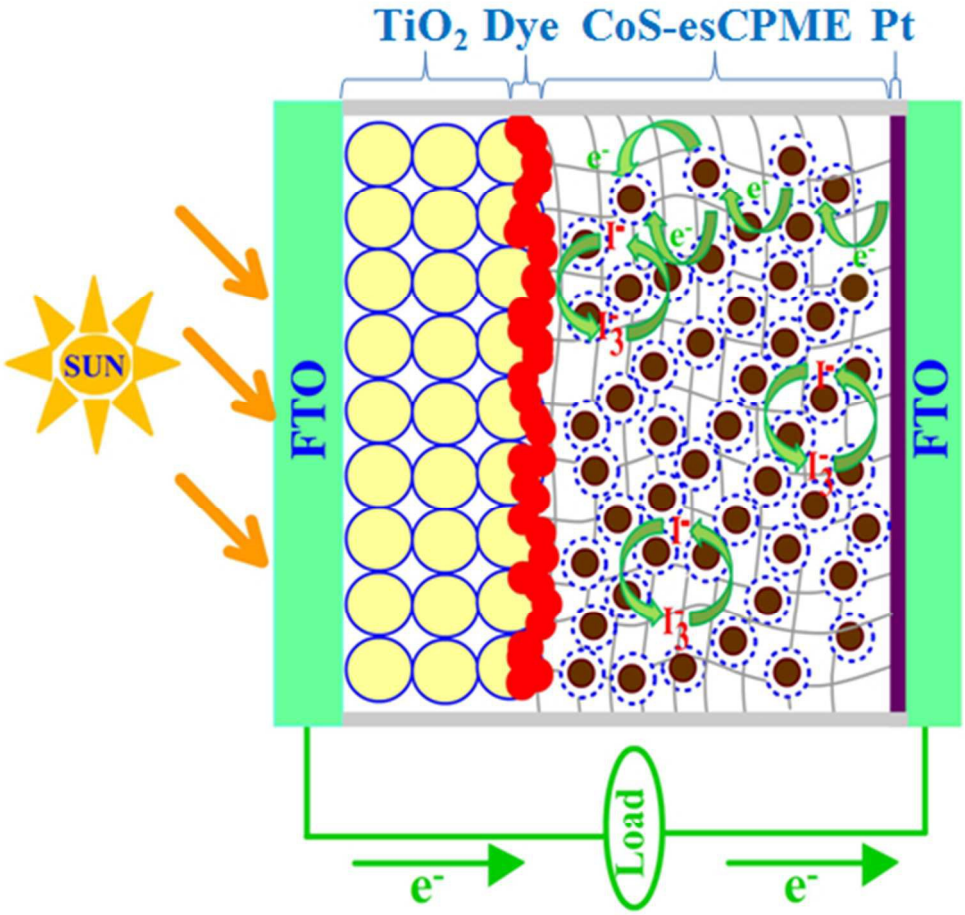

Fig. 9 Illustrates the mechanism of increased reaction kinetics of DSSC assembled using esCPME.
43x41mm (300 x 300 DPI)

View Article Online
DOI: 10.1039/C5RA04944J

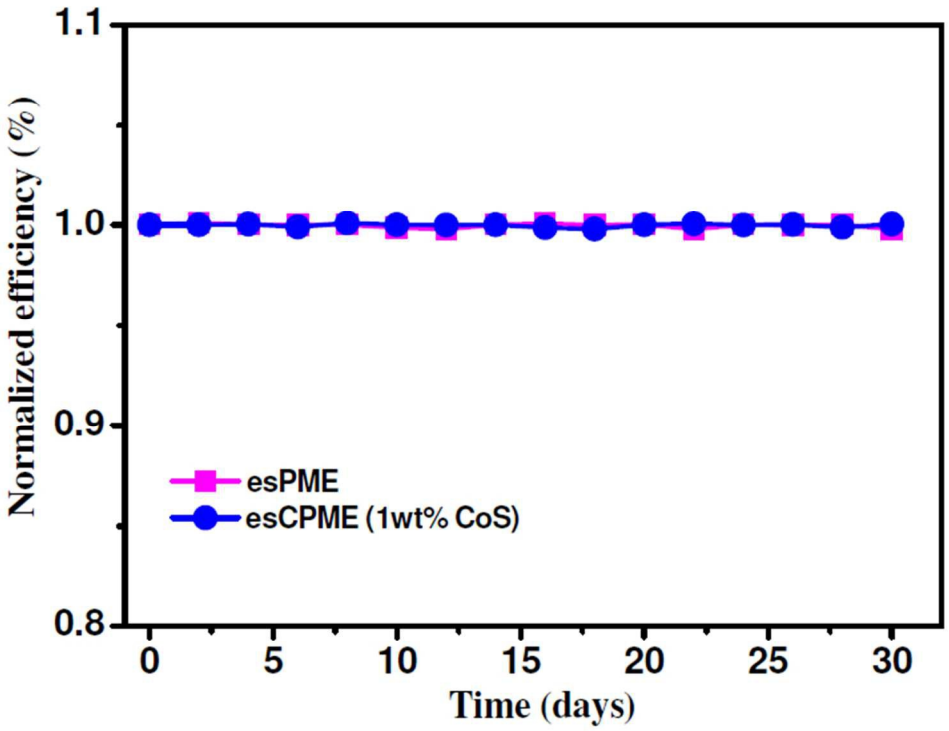

Fig. 10 Normalized efficiency of a) esPME and b) 1wt% of CoS incorporated esCPME.